Lasers in Medical Science (2025) 40:269
https://doi.org/10.1007/s10103-025-04507-7

RESEARCH

# Photobiomodulation in the parotid and submandibular glands: a Monte Carlo simulation of photon penetration using 525-nm, 660-nm, and 850-nm wavelengths

**Luciana Correa[1] · Lis Meirelles[1] · Regina Célia Gorni Carneiro[2] · Fábio Fernando Alves da Silva[2] · Eric L. Wisotzky[3] · Edouard Berrocal[4]**

Received: 1 October 2024 / Accepted: 30 May 2025


## Abstract

There are ongoing questions about the most effective wavelength for photobiomodulation (PBM) on major salivary glands due to the specific anatomical location and unique optical properties of the tissues surrounding the glands. The aim of this study was to analyze the photon propagation in the major salivary glands region of humans and rats using Monte Carlo (MC) stochastic simulation. Phantoms were designed to replicate the tissues surrounding the parotid and submandibular glands in humans and rats. Simulations were carried out using a MC online platform with wavelengths of 525 nm, 660 nm, and 850 nm. An experimental assay in rats was conducted to evaluate if the wavelength with the best performance could enhance the salivary flow. The 525 nm photons were primarily absorbed by the skin and fat tissue of humans and rats. Only in rats, this wavelength reached the salivary glands. The 660 nm photons reached the human glands but were more absorbed in the submandibular gland than in the parotid gland. The 850 nm photons had a higher absorption in both human and rat parotid glands. PBM using 850 nm wavelength improved the salivary flow in rats. The 660 nm and 850 nm wavelengths were more effectively absorbed in the human parotid and submandibular glands, respectively, compared to the 525 nm. The increased salivary flow observed in rats following treatment with 850 nm suggests a beneficial effect of this wavelength on salivary gland function.
**Clinical trial number:** Not applicable.

**Keywords** Monte Carlo simulation · Photobiomodulation · Salivary glands · Xerostomia

✉ Luciana Correa
lcorrea@usp.br

Lis Meirelles
lismeirelles@usp.br

Regina Célia Gorni Carneiro
reginagorni@usp.br

Fábio Fernando Alves da Silva
fabiofufg@gmail.com

Eric L. Wisotzky
eric.wisotzky@hhi.fraunhofer.de

Edouard Berrocal
edouard.berrocal@fysik.lu.se

[1] Universidade de São Paulo, São Paulo, Brazil

[2] Instituto de Pesquisas Energéticas e Nucleares, São Paulo, Brazil

[3] Fraunhofer Heinrich-Hertz-Institute HHI, Berlin, Germany

[4] Department of Physics, Lund University, Lund, Sweden

## Introduction

Xerostomia is characterized by a dry mouth sensation, often caused by a decrease in saliva production or changes in saliva composition. Factors such as radiation therapy in the head and neck area, chemotherapy, iodine therapy, autoimmune diseases, and certain medications can contribute to xerostomia, resulting in difficulties with speaking, chewing, and swallowing, ultimately impacting quality of life [1–3]. Changes in the oral microbiome and an increased risk of opportunistic infections in the mouth are also common in individuals with xerostomia [4]. Currently, there are no standardized protocols for preventing or treating hyposalivation and xerostomia, with most therapies being based on empirical evidence rather than robust scientific research.

One of the therapies involves photobiomodulation (PBM) with low-power lasers for intra and extra oral

Published online: 11 June 2025

irradiation. Clinical trials and meta-analyses have demonstrated the benefits of PBM in preventing salivary flow reduction caused by cancer treatment and medications in major salivary gland dysfunction (Table 1). A recent meta-analysis [13] confirmed these benefits, but the optimal PBM protocol remains uncertain. There are ongoing questions about the most effective wavelength and dosage considering the specific anatomical location and unique optical properties of the tissues surrounding the glands.

One method for studying photon absorption and scattering in multi-layered tissue is through Monte Carlo (MC) simulation, a stochastic modeling technique used to analyze photon propagation in tissue. This approach has been employed in the medical field since the 1980s [14, 15]. MC simulations have shown good reproducibility in clinical scenarios involving soft tissues near the oral cavity [16], making them a valuable tool for planning photobiomodulation protocols. Several open-source codes and programs have been developed [17] to model more complex scenarios, such as multi-layered phantoms with varying optical properties in each layer [18]. Recently, user-friendly web-based platforms have been introduced, allowing non-coders to easily model and visualize photon transport, absorption, and scattering in 3D multi-layered tissue simulations [19–22]. These systems often utilize computer networks with GPUs and CUDA to accelerate calculations and overcome time constraints [21, 23, 24].

This study was conducted to investigate the optimal wavelength for penetration and absorption in the parotid and submandibular glands, based on the benefits observed in clinical trials for xerostomia prevention and recovery. Utilizing a web-based Monte Carlo simulation platform [21], we simulated the anatomical characteristics of the parotid and submandibular glands in humans and rats, including tissue type and thickness. We tested a range of wavelengths reported in the literature (Table 1) to determine which wavelength had the highest likelihood of reaching the salivary glands. Additionally, we assessed whether the selected wavelength had any impact on salivary flow using a rat experimental model.

## Methods

### Ethics considerations

This study had already been approved by the Human and Animal Ethics Committee of our institution (Project no. 33/22).

### Anatomic measurements

To create the phantom for simulation, head and neck computerized tomography scans of 40 oncologic male patients aged 39 to 72 were obtained from The Cancer Genome Atlas Head-Neck Squamous Cell Carcinoma Collection [25] via the Cancer Imaging Archive [26]. The tissue layers in the region of the parotid and submandibular glands (Fig. 1A) were used for the construction. Sublingual gland was excluded due to its anatomical location requiring an intraoral PBM which was not the focus of this study. PBMT for these salivary glands is usually administered in the floor of the mouth, where the only tissue barrier is the oral mucosa, and the parameters commonly used are infrared wavelengths typical of oral PBMT protocols.

Measurements were conducted in the CT scans to determine the distances from the skin surface to the outer boundaries of the parotid and submandibular glands. This enabled the calculation of the thickness of the tissue layers in this area (Fig. 1C and D). The distances were obtained using a

**Table 1** Examples of extraoral photobiomodulation parameters used in clinical trials for the prevention and treatment of Xerostomia

| Ref | *N* | FBM Protocol | Region exposed to FBM |
|---|---|---|---|
| [5] | 34 | InGaAIP Laser, 780 nm, 15mW, 0.04 cm2 spot area, 10s, 3.8 J/cm2 per point | Bilateral parotid (6 points), bilateral submandibular (colon) |
| [6] | 21 | HeNe laser, 630 nm, 30mW, 2,5 a 3,8 J/cm2 | *P*arotid and bilateral submandibular (without specification of points) |
| [7] | 21 | 810 nm, 40 mW, 25 J/cm$^2$ 3x/sem. During radiotherapy. | *P*arotid (6 points), submandibular (3 points on each side) |
| [8] | 23 | 830 nm, 30mW, 0.028 cm² spot area,10s, 7.5 J/cm$^2$ 3x/no alternate days during radiotherapy | Parotid (6 points), submandibular (3 points on each side) |
| [9] | 37 | InGaAIP Laser 810 nm, 200mW, 0.028cm$^2$ spot, 4s per point, 0.8 J per point, 2.85 J/cm$^2$, 45.6 J/cm$^2$ total energy density, 714.2.mW/cm$^2$ 3x/week, four weeks | *P*arotid gland (3 points), submandibular gland (2 points), sublingual gland (1 point), buccal mucosa (2 points in each side) |
| [10] | 41 | 808 nm, 100mW, 0.028cm$^2$ spot, 40s and 4 J per point, 142 J/cm$^2$, 3.5 W/cm$^2$ | Parotid gland (6 points), submandibular gland (2 points) |
| [11] | 30 | 808 nm, 100mW, 4 J per point, 40.65 J/cm$^2$, 112 J 2-3x/week, 20 sessions | Parotid gland (8 points), submandibular gland (3 points) |
| [12] | 28 | 980 nm, 300mW, 20s, 6 J | Parotid gland (8 points), submandibular gland (2 points) |

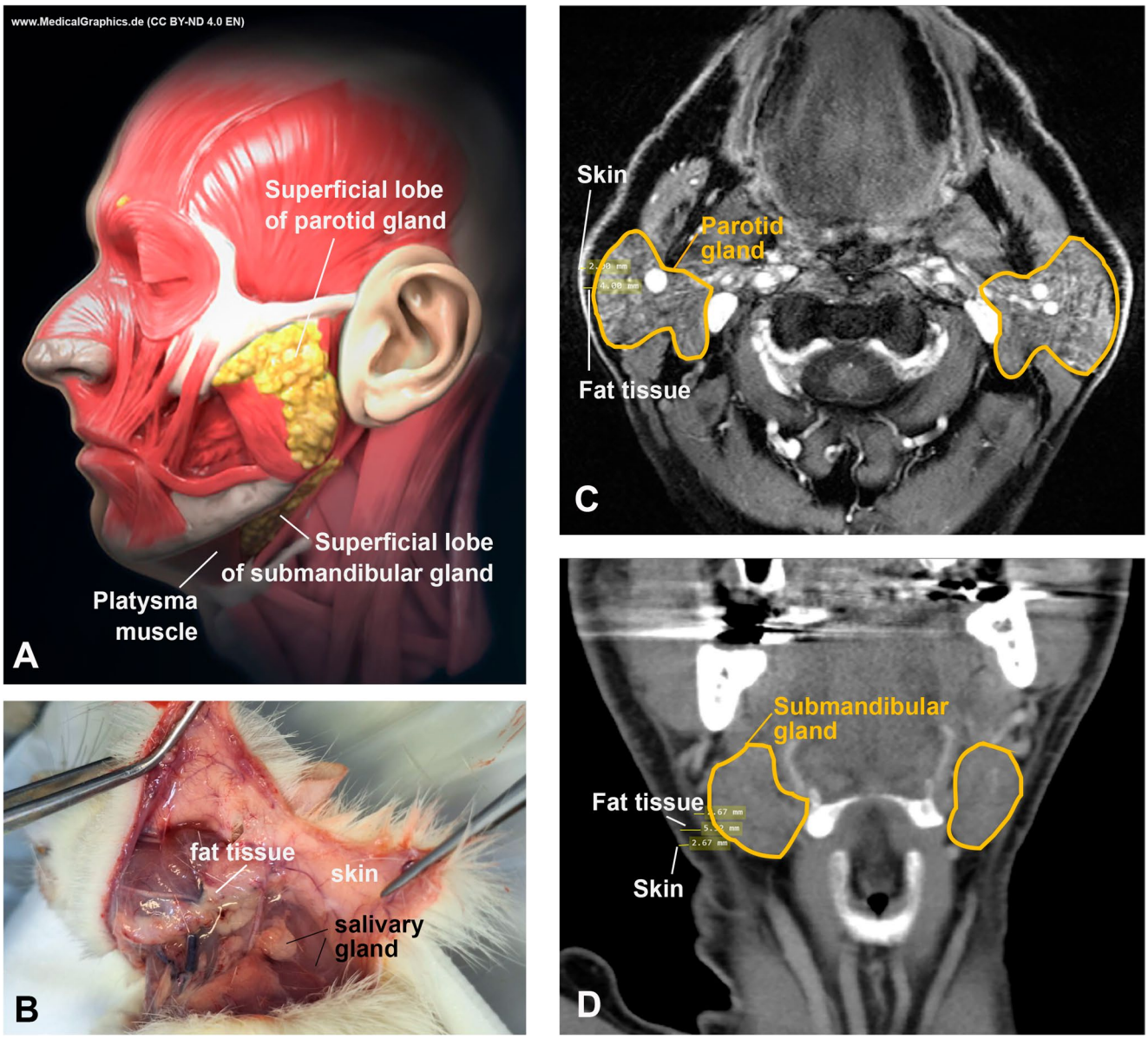


**Fig. 1** **A**: Anatomical positioning of human parotid and submandibular glands without skin and fat tissue. Only the superficial lobe of the glands was considered in the simulations. **B**: Anatomical positioning of rat parotid and submandibular glands, including the skin and fat tissue in the area. **C**: MRI scan (axial view) used to measure the thickness of skin and fat tissue around the human parotid gland (highlighted in yellow). **D**: MRI scan (coronal view) for measuring the thickness of skin, fat tissue, and platysma muscle around the human submandibular gland (highlighted in yellow)

measurement tool in an open-source software for DICOM image viewing and analysis (MicroDicom DICOM Viewer, Sofia, Bulgaria). The thickness for each tissue ranged as follows: parotid gland: skin– 1.8–2.2 mm; fat tissue– 2.6–3.7 mm; submandibular gland: skin– 2.2–2.8 mm; fat tissue– 4.5–7.8 mm; muscle– 2.1–2.3 mm.

In the rat simulation, the thickness of the skin and fat tissue around the parotid and submandibular glands was measured using a pachymeter during the euthanasia of rats in other experiments conducted at our institution (Fig. 1B). The depth of the fat tissue near the glands was also verified by measuring histological sections from the salivary glands. The skin and fat tissue thickness ranged from 0.5 to 1.5 mm and 1.8–2.3 mm, respectively, for both glands.

## Phantom design

Using the CT scan data, a phantom (Fig. 2) was created using the same software utilized for the Monte Carlo simulation (multi-scattering.com [21]). The scattering medium consisted of a $10 \times 10 \times 10$ voxel grid (each voxel measuring $1\text{mm}^3$). The human parotid region was modeled with

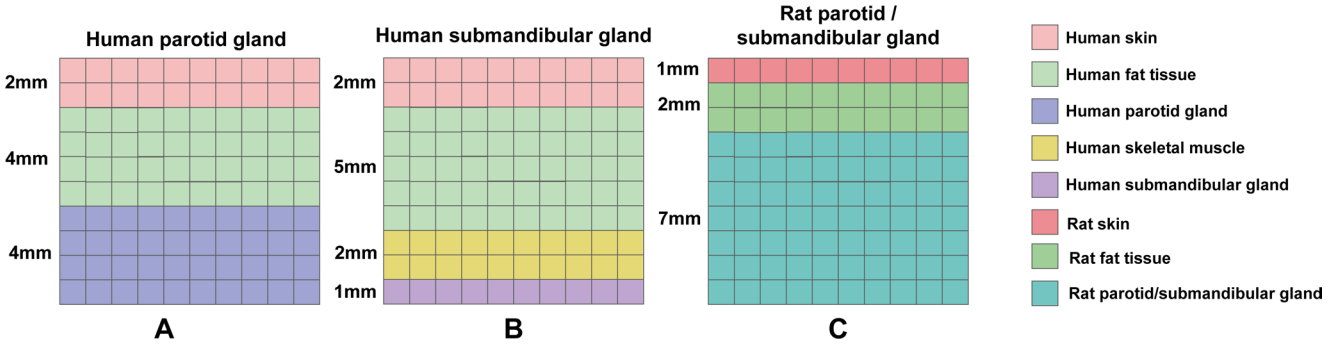


**Fig. 2** Schematic representation of the matrix containing 10 voxels (1mm3 per voxel) used for simulating each tissue layer in the human (**A** and B) and rat (**C**) major salivary glands region

**Table 2** Input values of optical properties for each tissue type in humans and rats used in the Monte Carlo simulation at the specified wavelength

| Layer | Absorption coefficient ($mm^{-1}$) | | Non-reduced Scattering coefficient ($mm^{-1}$) | |
|---|---|---|---|---|
| **525 nm** | **Human** | **Rat** | **Human** | **Rat** |
| Skin | 0.10 | 0.12 | 32.0 | 40.0 |
| Fat tissue | 0.39 | 0.05 | 14.2 | 12.0 |
| Parotid/submandibular gland | 1.32 | 1.32 | 33.6 | 33.6 |
| Muscle | 1.45 | - | 18.8 | - |
| **660 nm** | **Human** | **Rat** | **Human** | **Rat** |
| Skin | 0.06 | 0.06 | 20.0 | 25.0 |
| Fat tissue | 0.00 | 0.08 | 9.90 | 12.0 |
| Parotid/submandibular gland | 0.25 | 0.25 | 28.7 | 28.7 |
| Muscle | 0.12 | - | 11.5 | - |
| **850 nm** | **Human** | **Rat** | **Human** | **Rat** |
| Skin | 0.05 | 0.06 | 16.5 | 15.0 |
| Fat tissue | 0.00 | 0.10 | 9.2 | 12.0 |
| Parotid/submandibular gland | 0.09 | 0.09 | 25.0 | 25.0 |
| Muscle | 0.03 | - | 66.9 | - |

The optical properties for human tissue were sourced from: skin - Tseng et al. (2009) [28]; fat tissue, muscle, and parotid gland - Wisotzky et al. (2019) [27]. The optical properties for rat tissue were obtained from Bashkatov et al. (2000) [29]. As there were no available optical properties for rat parotid and submandibular gland in the literature, the values used were those adopted for human parotid gland

three layers: the first layer was skin (2 mm) in contact with the light beam, the second layer was fat tissue (4 mm), and the third layer was the parotid gland (4 mm, completing the phantom volume) (Fig. 2A). The human submandibular gland was also simulated with the same layers, but the fat tissue thickness was increased to 5 mm (considering the anatomic measurements described previously) and a 2 mm muscle layer was added to represent the platysma muscle (Fig. 2B). For the rat parotid and submandibular glands, a single phantom was used for all rat simulations due to the similarity in the anatomical region of both glands. The rat model included skin (1 mm), fat tissue (2 mm), and the glands (7 mm) as tissue layers (Fig. 2C).

## Monte Carlo simulations

We conducted Monte Carlo simulations using light sources with wavelengths of 660 nm and 850 nm, which are similar to those used in clinical trials involving photobiomodulation (PBM) on the major salivary glands (Table 1). Additionally, we examined the effects of 525 nm light, as the parotid gland has a high absorption coefficient for this wavelength [27]. The optical properties of each tissue layer in the human and rat phantoms were modeled based on literature values (Table 2). Since optical property values for submandibular glands were not available, we used the values for the parotid glands in our calculations. We believe that this limitation was partially mitigated by the fact that, under normal conditions, the superficial portions of both glands have a similar proportion of serous components [30]. As rat parotid and submandibular glands do not have distinct optical properties, the values used were the same as those for humans. The anisotropy coefficient (g) was set at 0.90. A light source resembling a laser probe with a 5 mm diameter and emitting $10^9$ photons was employed in the simulations. These parameters were determined based on the typical laser devices used in Dentistry for intra and extraoral irradiations. The source was placed perpendicular to the center of the phantom on the face corresponding to the y-axis. The algorithms applied in the simulations and validation of the software are detailed in previous studies [21, 31].

Z-axis images generated by the simulation platform were gathered to visually examine the propagation of photon packages on the phantom surface and the distribution of photon package weight within the phantom under each simulation condition. The total number of photons and average scattering number were also documented for comparison.

## Animal experiment for salivary flow analysis

We conducted an animal experimental assay to determine if the wavelength that performed better in the MC rat simulations would increase salivary flow. Twelve male Wistar

rats weighing 200 g were randomly assigned to two groups: Without PBM ($n=6$) - received no treatment; and with PBM ($n=6$)– exposed to PBM in the parotid and submandibular glands. The animals were kept in cages for 30 days, with consistent environmental conditions of temperature, humidity, and light-dark cycle. They had access to water and commercial food *ad libitum*.

PBM was conducted at two points in the parotid region on each side of the head, and at three points in the submandibular gland region (Fig. 3). The light parameters were selected to match the power and energy densities found in the literature (Table 1): 0.1 W, 0.2 W/cm$^2$, 0.5cm$^2$ spot area, 40s, 4 J, 8 J/cm$^2$. The 850 nm wavelength was selected because it penetrated deeper into the rat glands compared to other wavelengths in MC simulations, suggesting interaction with the surface of the glands (refer to Sect. 3.1 and 3.2 in the Results section, and Fig. 7). The PBM group underwent irradiation three times a week for four consecutive weeks after a brief sedation with isoflurane inhalation. The control group underwent the same sedation procedure but did not receive PBM.

Salivary flow was assessed at baseline (T0) and after 4 weeks of laser therapy (T1). The animals were anesthetized with isoflurane inhalation and then given an intraperitoneal injection of pilocarpine to stimulate salivary flow through activation of the parasympathetic system (10µL/g, 100 mg/kg total dose). A swab with a standardized volume was placed in the rat's oral cavity to collect saliva. After 15 min, the swab was removed, placed in a sterilized microtube, and stored at -8ºC until processing in the laboratory. Following centrifugation (5250 g for 4 min) and removal of the swab from the microtube, salivary flow (µL/min) was calculated by dividing the total saliva volume by 15 min. The salivary flow values at T1 were normalized to those at T0 (T1-T0) in both groups.

**Fig. 3** Application of photobiomodulation using an 850 nm LED probe on the cervical region of a rat. The circles indicate the points of illumination on the parotid and submandibular gland area

Salivary flow data were analyzed using the Shapiro-Wilks test, which indicated a non-parametric distribution. Wilcoxon's test was used for paired data comparisons between T0 and T1 within each group. Group comparisons were conducted using the Mann-Whitney test. The significance level was set at 0.05.

## Results

### Photons propagation in the phantom surface

The propagation of photons on the phantom surface differs significantly between human and rat tissues at different wavelengths (Fig. 4). Specifically, the 525 nm wavelength exhibited greater scattering patterns compared to 660 nm and 850 nm in both humans and rats. At 525 nm, photons were primarily concentrated in the skin for human. In contrast for rat, the photons were primarily concentrated in fat tissue and only a small number of photons is distributed in the thinner skin tissue. As the first two tissue layers are thinner for rat, some photons reached gland tissue.

The photons with a wavelength of 660 nm were found to be concentrated in the skin and particularly in the fat tissue for both species. In human tissues, more photons are dispersed in the first layer skin than in rat tissue. As well, the dissipation halos were more extended in human tissue for 660 nm compared to those observed within 525 nm. In contrast to the 525 nm simulations with human tissues where no photons reached the gland tissue layer, with 660 nm some photons reached parotid gland tissue. In the simulation involving the human submandibular gland, where the fat tissue layer was thicker (by 1 mm) and there was a muscle layer present, a minimal number of photons formed a halo that reached the muscle but did not reach the salivary gland. In rats, some photons at the 660 nm wavelength were also dispersed towards the salivary gland, but only in the superficial layer of the organ.

Like for 660 nm, in all simulations the 850 nm wavelength was found to penetrate deeper layers compared to the 525 nm simulations. Likewise, the 850 nm photons reached deeper layers for all rat and the human parotid gland simulations. In the human parotid gland, some photons were distributed in the superficial region of the gland, with the highest concentration observed in the skin and fat tissue. In the submandibular gland, the 850 nm photons did not accumulate in the gland region due to the presence of the muscle layer, resulting in a less prominent dissipation halo compared to the 660 nm wavelength in that area. The rat models exhibited a specific pattern of 850 nm photon distribution

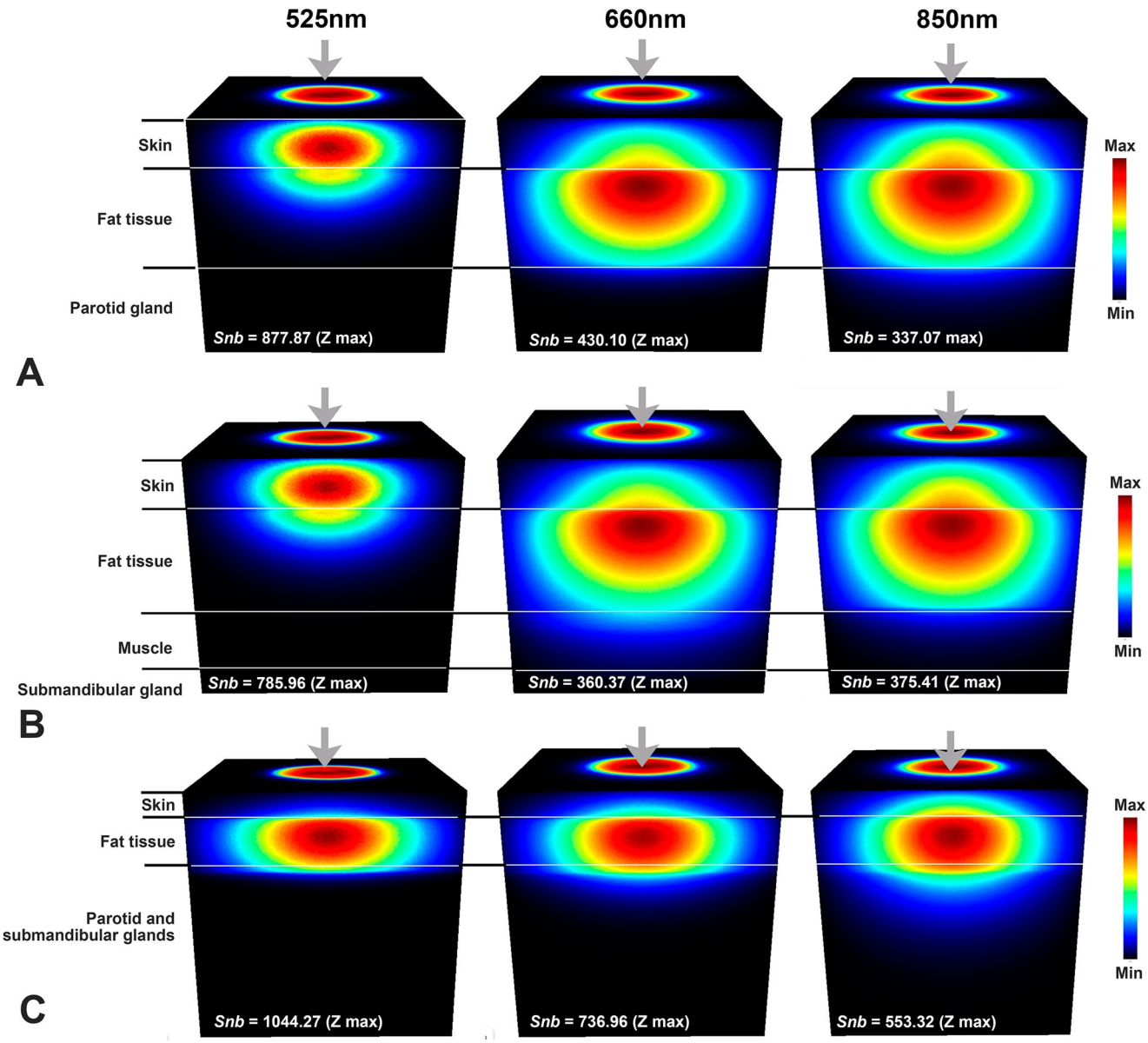


**Fig. 4** Distribution of photons in the parotid and submandibular salivary glands following Monte Carlo simulations with wavelengths of 525 nm, 660 nm, and 850 nm. The Z-axis is segmented into layers representing skin, fat tissue, muscle, and the parotid/submandibular glands in both human (**A** and **B**) and rat (**C**) models. *Snb* - average scattering number

in the superficial area of the parotid/submandibular glands, with the highest concentration also found in the skin and fat tissue.

## Scattering and absorption

In all simulations, photons were mainly absorbed by the skin, displaying distinct scattering and absorption patterns consistent with the particular wavelength employed.

At 525 nm (Fig. 5), the main absorption took place in the skin and fat tissue. There was no absorption of this wavelength in the human parotid and submandibular glands. Conversely, in rats, absorption was observed in the superficial part of the salivary glands with a relatively high intensity.

Photons at 660 nm (Fig. 6) and 850 nm (Fig. 7) wavelengths successfully reached the salivary gland layer in all the models. Both wavelengths exhibited significant absorption in the skin and absence of absorption in the fat tissue for human tissue. The 850 nm wavelength showed greater penetration in the parotid gland compared to the 660 nm wavelength in both humans and rats, indicating a pattern of increased photon penetration with longer wavelengths. In relation to the human submandibular gland, it was observed

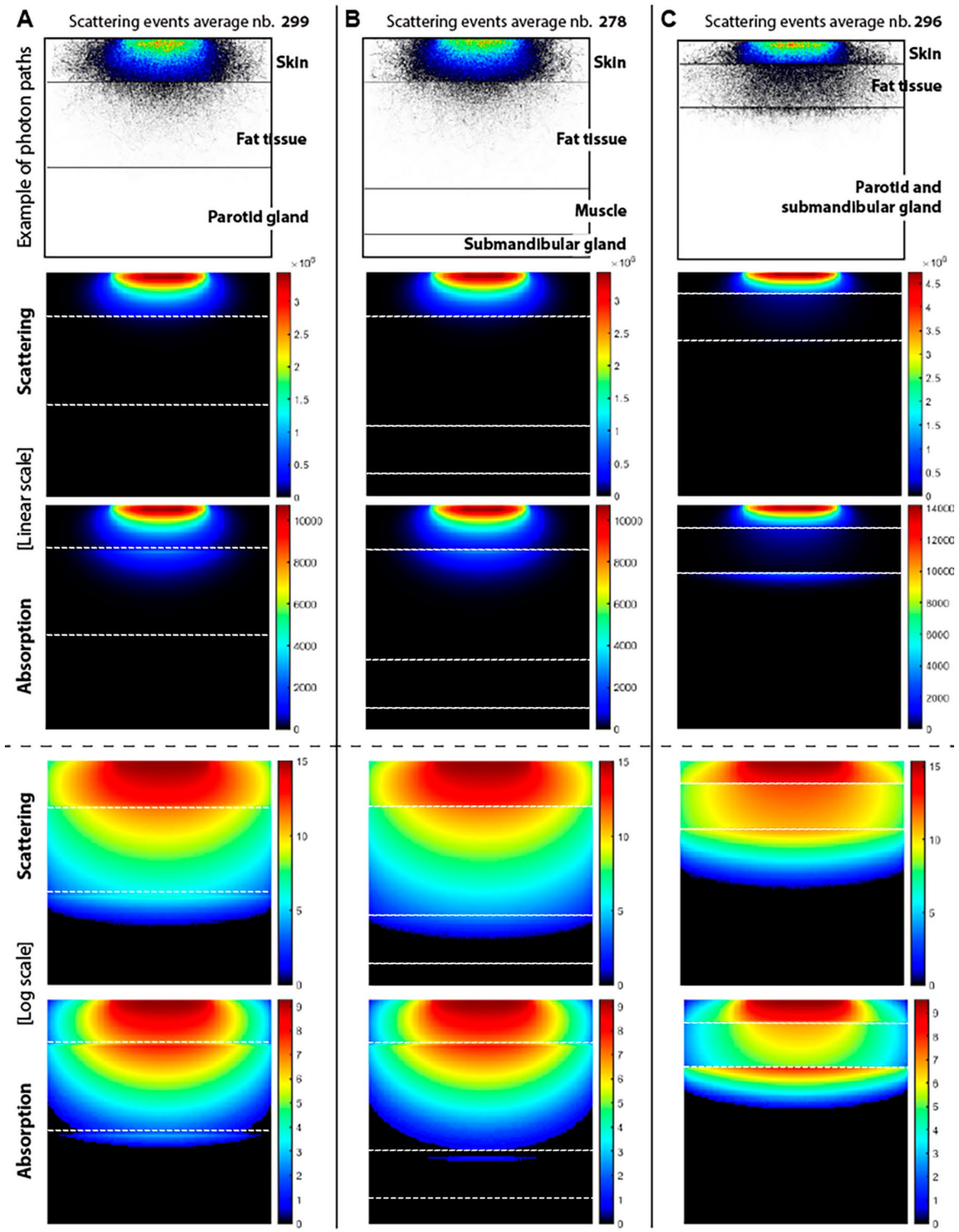


**Fig. 5** Linear and log scale values of scattering and absorption of 525 nm within the phantom and across different layers (skin, fat tissue, muscle, and salivary glands) in both human (**A**– parotid gland. **B**– submandibular gland) and rat (**C**– parotid and submandibular glands) models. White dot lines represent the tissue layers illustrated in the example of photons paths

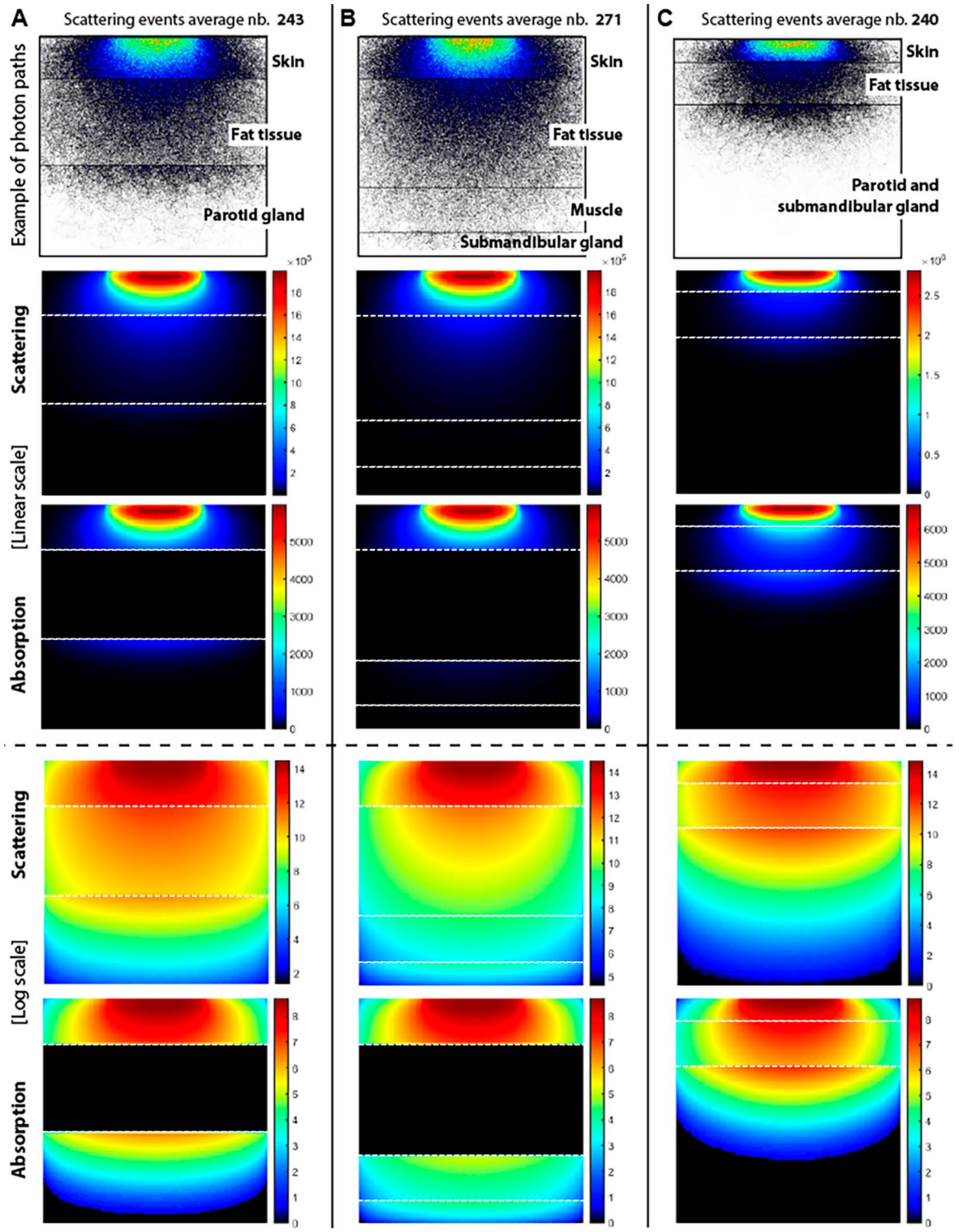


**Fig. 6** Linear and log scale values of scattering and absorption of 660 nm within the phantom and across different layers (skin, fat tissue, muscle, and salivary glands) in both human (**A**– parotid gland. **B**– submandibular gland) and rat (**C**– parotid and submandibular glands) models. White dot lines represent the tissue layers illustrated in the example of photons paths

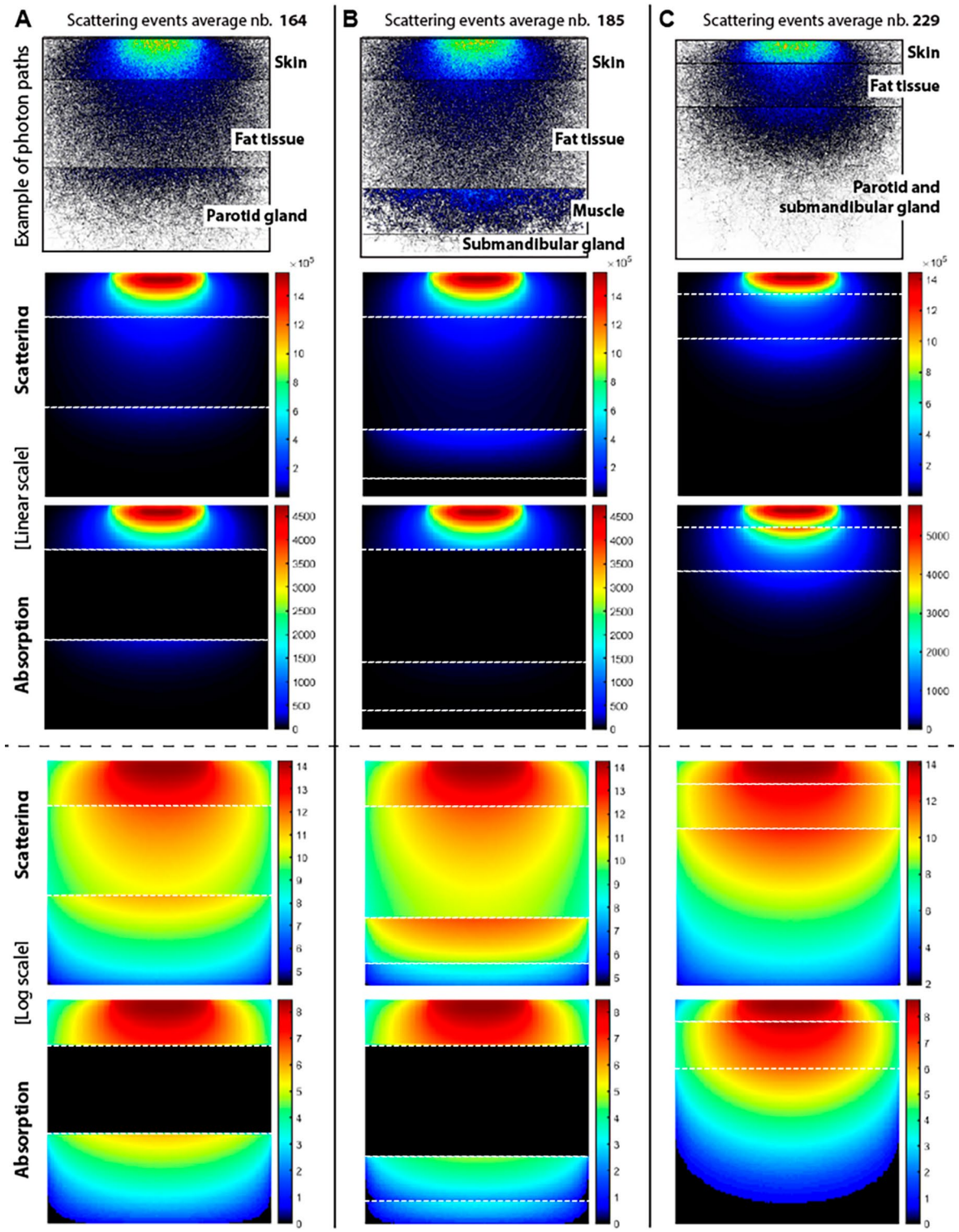


**Fig. 7** Linear and log scale values of scattering and absorption of 850 nm within the phantom and across different layers (skin, fat tissue, muscle, and salivary glands) in both human (**A**– parotid gland. **B**– submandibular gland) and rat (**C**– parotid and submandibular glands) models. White dot lines represent the tissue layers illustrated in the example of photons paths

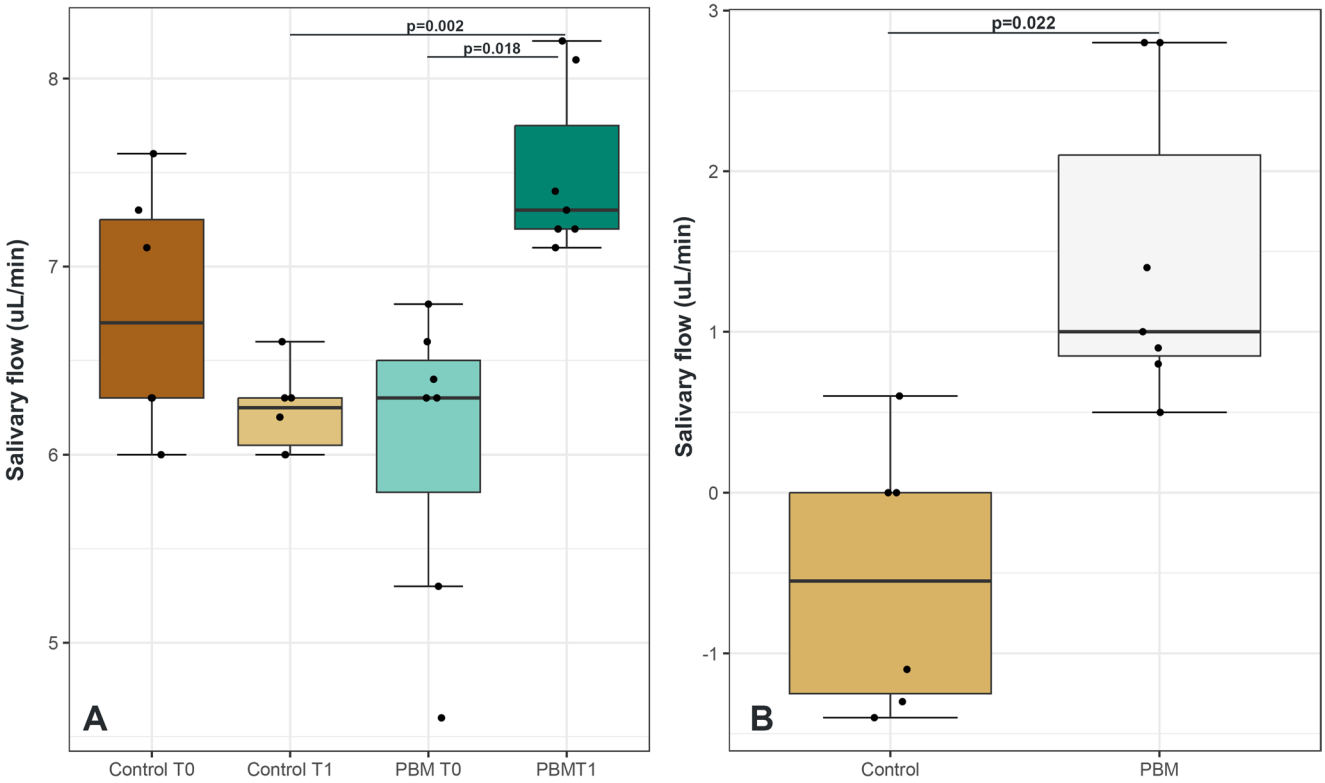


**Fig. 8** **A**: Comparison of salivary flow from the parotid and submandibular glands of rats in the PBM and Control groups at baseline (T0) and after 30 days of photobiomodulation (T1). The rats were exposed to light irradiation with a 850 nm wavelength twice a week for four weeks. P values were calculated using Wilcoxon´s test. **B**: Comparison of salivary flow after normalizing T1 values with T0. P values were calculated using the Mann-Whitney test. Whiskers represent the minimum and maximum values, box limits indicate the 25th and 75th quartiles, and the horizontal line in the box represents the median

that photons at 660 nm were absorbed to a greater extent than those at 850 nm, likely because of the varying scattering patterns in fat and muscle tissues at these two wavelengths.

### Salivary flow measurement

Based on the MC simulations in rats, the 850 nm wavelength demonstrated superior penetration into the deeper layers. Utilizing this wavelength, we performed a salivary flow measurement in normal rats. There were no significant differences between T0 and T1 in the control group. In the PBM group, there was a significant increase in salivary flow at T1 compared to T0 ($p=0.018$) (Fig. 8A). When comparing the two groups, the salivary flow was significantly higher in the PBM group than in the control group at T1 ($p=0.002$) (Fig. 8A). This trend was maintained after normalizing T1 with T0 (T1-T0) ($p=0.022$) (Fig. 8B).

## Discussion

One of the key considerations for extraoral PBM is determining the most suitable wavelength to target the parotid and submandibular glands, considering the potential interference of skin, fat tissue, and muscle that cover these glands. Despite the presence of these tissue layers, the parotid gland has a lobe that is near the skin surface, making it a superficial layer that is likely to be affected by light. However, the parotid gland has higher absorption and scattering coefficients in the 300 to 600 nm range [27], which overlaps with the wavelengths that are strongly absorbed and scattered by the skin and fat tissue surrounding the gland. This overlap limits the effectiveness of this wavelength range in interacting with the glands due to significant absorption in the superficial tissue layers.

We noticed this trend analyzing the 525 nm wavelength in the human model, which it was primarily absorbed in skin and fat tissue. While 525 nm light is well absorbed by the human parotid gland in direct measurements [27], it did not yield satisfactory results when covering tissues of at least 6 mm were included. Conversely, in rats, in which the tissue layers are thin (3 mm) and have different optical properties

compared to the human tissues, Monte Carlo simulations indicated high absorption of 525 nm light in the superficial region of the glands. Therefore, based on these simulations, we do not recommend using 525 nm for extraoral PBM in human parotid and submandibular glands. However, we suggest conducting tests with 525 nm light to assess its PBM effects on salivary glands in murine models.

The 660 nm and 850 nm wavelengths exhibited a similar pattern of photon absorption in the tissue layers, with high absorption in the dermis and some interaction with the glands in the human model. The wider photon spread of 850 nm made it a more favorable choice compared to 660 nm. In rats, both wavelengths reached the glands, but the 850 nm wavelength, with its broader spread, was deemed more advantageous. The lower absorption of these wavelengths by the skin and the absence of absorption in the fat tissue, compared to 525 nm, likely facilitated photon propagation into deeper layers. Research on PBM in the salivary glands has focused on wavelengths that are less absorbed by the skin and fat tissue. For example, in a clinical trial, the authors opted for the 980 nm wavelength to reduce xerostomia [12] based on the hypothesis that it would penetrate more effectively, thanks to low skin absorption, and have a greater interaction with water, which is an essential component for saliva production.

Compared to the parotid gland, the submandibular gland is less ideal for PBM due to its deeper location, thicker layer of fat tissue, and thin muscle covering the superficial lobe of the gland. However, in our Monte Carlo simulations, we found that the 660 nm and 850 nm wavelengths were able to reach the human submandibular gland, albeit with very low absorption levels. Analyzing the log data revealed that the 660 nm wavelength exhibited a higher level of absorption in the submandibular gland compared to the 850 nm wavelength. This difference is likely due to the higher scattering of the 850 nm wavelength in the muscle, causing a change in the photon trajectory within the submandibular layer. These findings support the use of the 660 nm wavelength in clinical studies targeting PBM for human submandibular glands.

One notable observation from the simulations was the impact of fat tissue on the penetration of photons into deeper layers. For instance, increasing the thickness of fat tissue by 1 mm in the human submandibular model resulted in a different distribution pattern of photons compared to the human parotid model. The low absorption and high scattering coefficients of fat tissue at 660 nm and 850 nm wavelengths may account for this observation. Studies and simulations on the optical properties of fat tissue have shown that the spherical shape of adipose cells contributes to the phenomenon of light reflectance known as a photonic jet, where each cell acts as a spherical microlens [32, 33]. This phenomenon could explain the variation in photon distribution mentioned earlier. Hence, when selecting wavelengths for PBM planning, it is essential to consider not just the absorption coefficients and thickness of the tissues in the targeted area, but also their morphological structure and reflective properties [33].

In the context of simulated tissues and chosen wavelengths, hemoglobin and water emerge as crucial chromophores [34]. The absorption coefficient is known to rise with the increase in blood vessel volume within the tissue, especially at 525–660 nm wavelengths [35, 36]. In this study, we assumed that all tissues were normal and did not exhibit vasodilation, edema, angiogenesis, or other factors that could affect blood flow in the microvasculature and tissue water content. However, PBM is commonly used on salivary glands in cases of xerostomia resulting from gland necrosis due to radiation or chemotherapy, leading to fibrosis of the glandular tissue, or in cases of sialadenitis caused by various factors (medication, autoimmune diseases, infections, etc.). The composition of water, collagen, and hemoglobin in the salivary gland and surrounding tissues in these conditions may differ from those considered in this study and may alter the trends described in the current results.

In the rat model, there was low photon absorption in the layer of the parotid/submandibular gland. However, the 850 nm wavelength, which allowed for better photon penetration, improved salivary gland function after four weeks of PBM application. Factors such as stimuli in sympathetic and parasympathetic nerves, mastication movements, and water transport from blood to secretory portion of the gland play crucial roles in saliva production [37]. While direct photon interaction with the glands was not prominently detected, the positive effect on salivation likely resulted from an indirect effect of PBM, possibly related to nerve and blood flow stimulation localized in the dermis and fat tissue. In addition, the PBM regimen with multiple points and high energy density used in the rat experimental model may contribute for stimulating salivary flow. While there are anatomical and physiological differences between human and rat salivary glands, the indirect impact of PBM could potentially influence saliva production in humans as well. Indeed, research has demonstrated a beneficial effect of PBM on salivary flow in patients, as evidenced by clinical studies [13], though further substantial scientific proof is required.

## Limitations of the study

This study is limited in several ways. In addition to the limitations mentioned earlier, another limitation is the lack of simulations considering variations in skin composition, particularly in terms of hemoglobin and melanin pigments. Variations in the distribution of these components can

affect optical properties and have a significant impact on the results [36]. To address potential inaccuracies in measurements, we used absorption and scattering coefficients obtained from in vivo studies in human and rat species, taking into account factors such as physiological temperature and blood flow [33, 38]. We did not account for scenarios where obese patients are exposed to light, which could alter photon scattering due to thicker fat tissue [33]. Additionally, we lacked absorption and scattering values specific to the submandibular gland. We used values from the parotid gland as a proxy, despite differences in gland composition and vascularity, which could affect tissue optical properties [39].

## Conclusions

MC simulations of the tissue layers that cover the parotid and submandibular glands in humans and rats showed that photons at 660 nm and 850 nm wavelengths had better penetration compared to those at 525 nm. The 850 nm showed a higher penetration than 660 nm in the human parotid gland, whereas the 660 nm wavelength was more absorbed by the human submandibular glands. A 4-week PBM treatment using 850 nm improved salivary flow in a rat model, indicating a positive impact of this wavelength on salivary gland function. Future Monte Carlo simulations could be conducted using more intricate phantoms that accurately replicate the anatomy of nerves and blood vessels in both normal and altered salivary glands to enhance PBM clinical protocols.

**Author contributions** Conceptualization: LC, EB; Formal analysis: LC, EB, ELW; Funding acquisition: LC; Methodology: LM, RCGC, FFAS; Software: EB; Visualization: EB, LC; Writing (original draft): LC; Writing (review and editing): all.

**Funding** This work was supported by the São Paulo Research Foundation (FAPESP) [grant number 2023/03299-9]; and in part by the Coordenação de Aperfeiçoamento de Pessoal de Nível Superior– Brasil (CAPES) [grant number 001].

**Data availability** Raw data are available and can be solicited to the corresponding author.

## Declarations

**Competing interests** The authors declare no competing interests.

## References

1. Gunning JA, Limesand KH, Chronic Phenotypes Underlying Radiation-Induced Salivary Gland Dysfunction (2024) J Dent Res 29:220345241252396. https://doi.org/10.1177/00220345241252396
2. Kakei Y, Shimosato M, Soutome S, Funahara M, Shikama Y, Sakamoto Y, Ikegami Y, Otsuru M, Natsume N, Umeda M (2024) Interventional prospective studies on Xerostomia in patients undergoing palliative and End-of-Life care. Scoping Rev Cureus 16:e63002. https://doi.org/10.7759/cureus.63002
3. Song EC, Chung SH, Kim JH (2024) Molecular mechanisms of saliva secretion and hyposecretion. Eur J Oral Sci 132:e12969. https://doi.org/10.1111/eos.12969
4. Nagakubo D, Kaibori Y (2023) Oral microbiota: the influences and interactions of saliva, iga, and dietary factors in health and disease. Microorganisms 11:2307. https://doi.org/10.3390/microorganisms11092307
5. Gonnelli FA, Palma LF, Giordani AJ, Deboni AL, Dias RS, Segreto RA, Segreto HR (2016) Low-Level laser for mitigation of low salivary flow rate in head and neck Cancer patients undergoing radiochemotherapy: A prospective longitudinal study. Photomed Laser Surg 34:326–330. https://doi.org/10.1089/pho.2016.4104
6. Libik TV et al (2017) Management of cancer therapy-induced oral mucositis pain and xerostomia with extra- and intra oral laser irradiation. AIP Conference Proceedings 1882, 020044. https://doi.org/10.1063/1.5001623
7. Louzeiro GC, Cherubini K, de Figueiredo MAZ, Salum FG (2020) Effect of photobiomodulation on salivary flow and composition, Xerostomia and quality of life of patients during head and neck radiotherapy in short term follow-up: A randomized controlled clinical trial. J Photochem Photobiol B 209:111933. https://doi.org/10.1016/j.jphotobiol.2020.111933
8. Ribeiro LN, Lima MH, Carvalho AT, Albuquerque RF, Leão JC, Silva IH (2021) Evaluation of the salivary function of patients in treatment with radiotherapy for head and neck cancer submitted to photobiomodulation. Med Oral Patol Oral Cir Bucal 26:e14–e20. https://doi.org/10.4317/medoral.23912
9. Mosannen Mozaffari P, Delavarian Z, Fekrazad R, Fani Pakdel A, Rashed Mohassel M, Taghi Shakeri M, Ghazi A (2024) Evaluation of the effect of photobiomodulation on Radiation-Induced Xerostomia in head and neck Cancer patients: A randomized clinical trial. J Lasers Med Sci 15:e4. https://doi.org/10.34172/jlms.2024.04
10. Varellis MLZ, Bussadori SK, Pavesi VCS, Pereira BJ, Bezerra CDS, Silva FG, Castro GS, Afonso RCT, Barbosa Filho VF, Deana AM (2024) Evaluation of photobiomodulation in the salivary production of patients with hyposalivation induced by antihypertensive drugs - A blind, randomized, controlled clinical trial. Complement Ther Clin Pract 56:101845. https://doi.org/10.1016/j.ctcp.2024.101845
11. Schepanski N, Costa FS, Machado EFM, Pacheco MN, Amaral CDB, Machado RC, Nogueira ARA, Brancher JA, Sassi LM, de Araujo MR (2024) Evaluation of photobiomodulation therapy (PBMT) on salivary flow and composition in head and neck cancer patients undergoing radiation therapy. Oral Surg Oral Med Oral Pathol Oral Radiol 137:253–263. https://doi.org/10.1016/j.oooo.2023.11.007
12. Derikvand N, Basirat M, Ghasemi SS, Hashemi R (2023) The photobiomodulation effect of 980 Nm diode laser on patients with Xerostomia. Lasers Med Sci 39:10. https://doi.org/10.1007/s10103-023-03949-1
13. Oliveira SV, Batista JVF, Gutierres GG, Silva NP, Lino-Dos-Santos-Franco A, Rodrigues MFSD, Cecatto RB (2024) The supportive use of photobiomodulation on salivary glands: a narrative review and meta-analysis. Eur Arch Otorhinolaryngol 281(6):2793–2805. https://doi.org/10.1007/s00405-023-08425-8

14. Wilson BC, Adam G (1983) A Monte Carlo model for the absorption and flux distributions of light in tissue. Med Phys 10(6):824–830. https://doi.org/10.1118/1.595361
15. Jacques SL, Alter CA, Prahl SA (1987) Angular dependence of HeNe laser light scattering by human dermis. Lasers Life Sci 1:309–334
16. Yaroslavsky AN, Juliano AF, Adnan A, Selting WJ, Iorizzo TW, Carroll JD, Sonis ST, Duncan CN, London WB, Treister NS (2021) Validation of a Monte Carlo modelling based dosimetry of extraoral photobiomodulation. Diagnostics (Basel) 11(12):2207. https://doi.org/10.3390/diagnostics11122207
17. Jacques SL (2022) History of Monte Carlo modeling of light transport in tissues using mcml.c. J Biomed Opt 27:083002. https://doi.org/10.1117/1.JBO.27.8.083002
18. Wang L, Jacques SL, Zheng L (1995) MCML—Monte Carlo modeling of light transport in multi-layered tissues. Comput Methods Programs Biomed 47:131–146. https://doi.org/10.1016/0169-2607(95)01640-f
19. Fang Q, Boas DA (2009) Monte Carlo simulation of photon migration in 3D turbid media accelerated by graphics processing units. Opt Express 17(22):20178–20190. https://doi.org/10.1364/OE.17.020178
20. Doronin A, Meglinski I (2011) Online object oriented Monte Carlo computational tool for the needs of biomedical optics. Biomed Opt Express 2:2461–2469. https://doi.org/10.1364/BOE.2.002461
21. Jönsson J, Berrocal E (2020) Multi-Scattering software: part I: online accelerated Monte Carlo simulation of light transport through scattering media. Opt Express 28:37612–37638. https://doi.org/10.1364/OE.404005
22. Hayakawa CK, Malenfant L, Ranasinghesagara J, Cuccia DJ, Spanier J, Venugopalan V (2022) MCCL: an open-source software application for Monte Carlo simulations of radiative transport. J Biomed Opt 27:083005. https://doi.org/10.1117/1.JBO.27.8.083005
23. Alerstam E, Svensson T, Andersson-Engels S (2008) Parallel computing with graphics processing units for high-speed Monte Carlo simulation of photon migration. J Biomed Opt 13:060504. https://doi.org/10.1117/1.3041496
24. Ren N, Liang J, Qu X, Li J, Lu B, Tian J (2010) GPU-based Monte Carlo simulation for light propagation in complex heterogeneous tissues. Opt Express 18:6811–6823. https://doi.org/10.1364/OE.18.006811
25. Zuley ML, Jarosz R, Kirk S, Lee Y, Colen R, Garcia K, Delbeke D, Pham M, Nagy P, Sevinc G, Goldsmith M, Khan S, Net JM, Lucchesi FR, Aredes ND (2016) The Cancer Genome Atlas Head-Neck Squamous Cell Carcinoma Collection (TCGA-HNSC) (Version 5) [Data set]. The Cancer Imaging Archive. https://doi.org/10.7937/K9/TCIA.2016.LXKQ47MS
26. Clark K, Vendt B, Smith K, Freymann J, Kirby J, Koppel P, Moore S, Phillips S, Maffitt D, Pringle M, Tarbox L, Prior F (2013) The Cancer imaging archive (TCIA): maintaining and operating a public information repository. J Digit Imaging 26:1045–1057. https://doi.org/10.1007/s10278-013-9622-7
27. Wisotzky EL, Uecker FC, Dommerich S, Hilsmann A, Eisert P, Arens P (2019) Determination of optical properties of human tissues obtained from parotidectomy in the spectral range of 250 to 800 Nm. J Biomed Opt 24:1–7. https://doi.org/10.1117/1.JBO.24.12.125001
28. Tseng SH, Bargo P, Durkin A, Kollias N (2009) Chromophore concentrations, absorption and scattering properties of human skin in-vivo. Opt Express 17:14599–14617. https://doi.org/10.1364/oe.17.014599
29. Bashkatov AN, Genina EA, Korovina IV, Kochubey VI, Sinichkin YP, Tuchin VV (2000) In vivo and in vitro study of control of rat skin optical properties by acting of osmotical liquid. Proceedings of SPIE 4224: 300–311. https://doi.org/10.1117/12.403935
30. Martinoli C, Derchi LE, Solbiati L, Rizzatto G, Silvestri E, Giannoni M (1994) Color doppler sonography of salivary glands. AJR Am J Roentgenol 163:933–941. https://doi.org/10.2214/ajr.163.4.8092039
31. Frantz D, Jönsson J, Berrocal E (2022) Multi-scattering software part II: experimental validation for the light intensity distribution. Opt Express 30:1261–1279. https://doi.org/10.1364/OE.445394
32. Bykov A, Tuchin V, Meglinski I (2022) Multiplexed spatially-focused localization of light in adipose biological tissues. Sci Rep 12:9711. https://doi.org/10.1038/s41598-022-14350-3
33. Yanina IY, Dyachenko PA, Abdurashitov AS, Shalin AS, Minin IV, Minin OV, Bulygin AD, Vrazhnov DA, Kistenev YV, Tuchin VV (2023) Light distribution in fat cell layers at physiological temperatures. Sci Rep 13:1073. https://doi.org/10.1038/s41598-022-25012-9
34. Mühle R, Markgraf W, Hilsmann A, Malberg H, Eisert P, Wisotzky EL (2021) Comparison of different spectral cameras for image-guided organ transplantation. J Biomed Opt 26:076007. https://doi.org/10.1117/1.JBO.26.7.076007
35. Lister T, Wright PA, Chappell PH (2012) Optical properties of human skin. J Biomed Opt 17:90901–90901. https://doi.org/10.1117/1.JBO.17.9.090901
36. Jacques SL (2013) Optical properties of biological tissues: a review. Phys Med Biol 58:R37–61. https://doi.org/10.1088/0031-9155/58/11/R37
37. Proctor GB (2016) The physiology of salivary secretion. Periodontol 2000 70:11–25. https://doi.org/10.1111/prd.12116
38. Setchfield K, Gorman A, Simpson AHRW, Somekh MG, Wright AJ (2023) Relevance and utility of [invited]he *[invited]n-vivo* and *[invited]x-vivo* optical properties of [invited]he skin reported [invited]n [invited]he literature: a review [Invited]. Biomed Opt Express 14:3555–3583. https://doi.org/10.1364/BOE.493588
39. Ustabaşıoğlu FE, Korkmaz S, İlgen U, Solak S, Kula O, Turan S, Emmüngil H (2020) Quantitative assessment of salivary gland parenchymal vascularization using power doppler ultrasound and Superb microvascular imaging: A potential tool in the diagnosis of sjögren's syndrome. Balkan Med J 37:203–207. https://doi.org/10.4274/balkanmedj.galenos.2020.2019.11.91